ELSEVIER

Journal of Nuclear Materials 245 (1997) 87–107

journal of nuclear materials

Review

Radiation resistant ceramic matrix composites

R.H. Jones [a,*], D. Steiner [b], H.L. Heinisch [a], G.A. Newsome [c], H.M. Kerch [d]

[a] *Pacific Northwest National Laboratory, PO Box 999, Richland, WA 99352, USA*
[b] *Department of Environmental and Energy Engineering, Rensselaer Polytechnic Institute, Troy, NY 12180-3590, USA*
[c] *Knolls Atomic Power Laboratory, PO Box 1072, Schenectady, NY 12301-1072, USA*
[d] *Office of Basic Energy Sciences, Division of Materials Sciences, US Department of Energy, ER-131, Germantown, MD 20874-1290, USA*

Received 16 February 1996; accepted 11 March 1997

Abstract

Ceramic matrix composites are of interest for nuclear applications because of their high-temperature properties, corrosion resistance, fracture toughness relative to monolithic ceramics, and low neutron activation and after heat. Evaluations of the radiation resistance of commercially available SiC/SiC composites have revealed their promise for this application, but also the need for further development to achieve the desired performance. This paper summarizes the results of a workshop cosponsored by the Offices of Fusion Energy and Basic Energy Sciences of the US Department of Energy and Lockheed–Martin Corporation with forty attendees from national laboratories, universities and industry. A number of promising routes for optimizing the radiation stability of ceramic matrix composites were identified at this workshop. These routes included the newer, more stoichiometric fibers and alternate fiber/matrix interfaces and matrix processing routes.

1. Introduction

Ceramic matrix composites, such as SiC/SiC, offer the potential of radiation resistant, high-temperature materials for nuclear environments. This potential relies in part on their high-temperature strengths, corrosion resistance, and thermal stability coupled with useful fracture toughness. Radiation resistance may be possible if the components comprising the composite exhibit radiation resistance. In the case of SiC_f/SiC composites, if the radiation resistance of beta SiC is achieved in the fiber, matrix and fiber/matrix interphase then a radiation resistant composite is possible.

A workshop entitled, 'Radiation Resistant Ceramic Matrix Composites', was held at Rensselaer Polytechnic Institute (RPI), July 11–13, 1994, to evaluate the status and developmental issues associated with application of ceramic composites in nuclear environments. The Workshop had three goals: (1) to exchange information among several programs involved in the development of radiation resistant ceramic matrix composites; (2) to identify routes for improving the radiation resistance of SiC/SiC and (3) to identify collaborative efforts that can focus and accelerate the development effort.

The purpose of this paper is to summarize the status of ceramic matrix composite development for radiation resistance as discussed at the Workshop. Section 2 describes the application of SiC/SiC composites in fusion energy systems. Section 3 discusses SiC/SiC properties, highlighting critical properties and key issues. Section 4 provides a status summary on the fundamental aspects of radiation damage in SiC and the radiation performance of SiC and SiC/SiC composites. Section 5 examines fiber/interface/matrix options for nuclear applications, including considerations of matrix processing routes and fiber architecture. Section 6 summarizes major conclusions, key issues and future directions.

2. A potential application of SiC/SiC

A thorough discussion of SiC/SiC composite applications in a radiation environment can be found in reports

* Corresponding author. Tel.: +1-509 376 4276; fax: +1-509 376 0418; e-mail: rh_jones@pnl.gov.

PII S0022-3115(97)00022-6

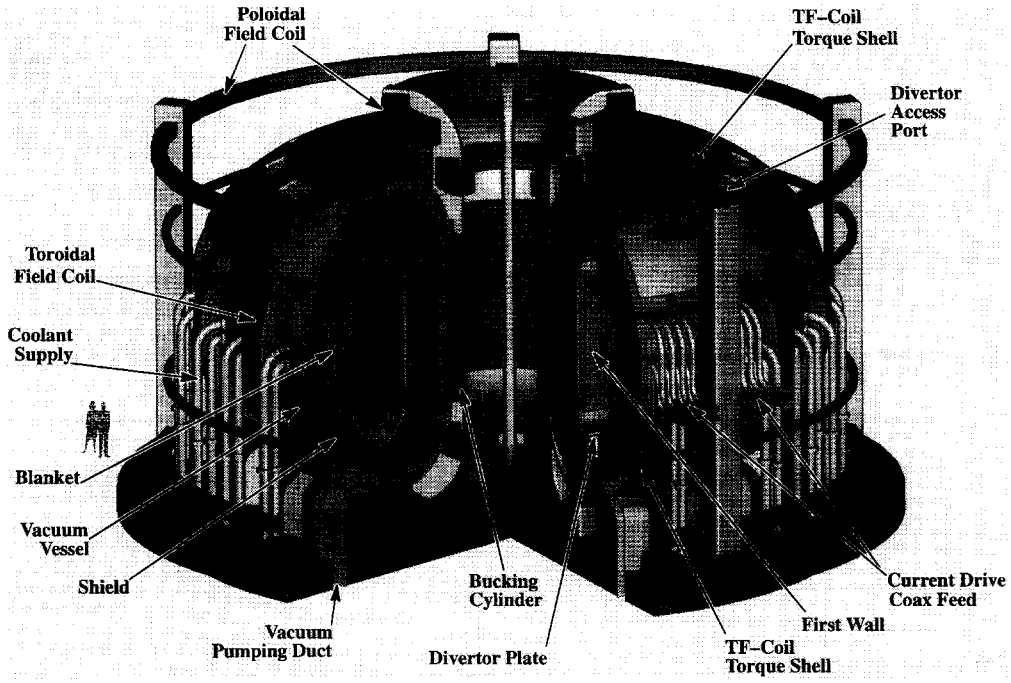

Fig. 1. Conceptual design for ARIES-I Tokamak.

describing the ARIES-I Tokamak reactor study [1]. The ARIES study examined four concepts of Tokamak Fusion Power Systems and was undertaken to: (1) determine the economic, safety and environmental potential of Tokamak fusion power systems, and (2) identify physics and technology areas with the highest leverage for achieving attractive fusion power plants. ARIES-I, the first of the ARIES concepts, is based on a modest extrapolation from the present Tokamak physics data base. The design relies on technologies that have been, at a minimum, already demonstrated in the laboratory and could be brought to an engineering standard on a time scale of 20 years.

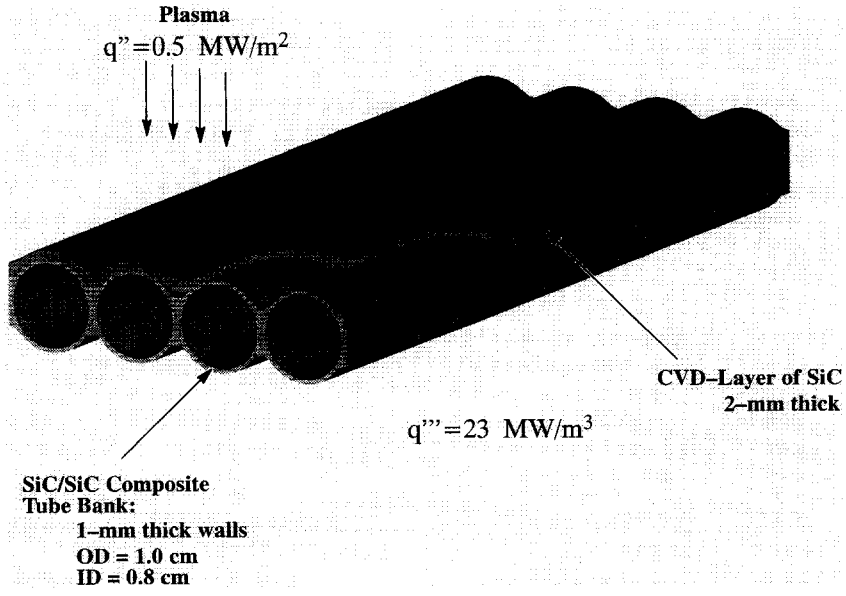

Fig. 2. Detail of first wall design for ARIES-I.

The ARIES-I conceptual design is depicted in Fig. 1. The energy source is based on the fusion of deuterium and tritium (D and T) and the system is designed to produce 1000 MW_l. Each D–T fusion event produces a 14.1 MeV neutron and a 3.5 MeV alpha particle. The fusion neutrons are very penetrating and result in neutron fluxes throughout the bulk of all major components, e.g., the first wall, blanket, shield and divertor plate. The energetic alpha particles deposit most of their energy in the plasma. Energy leaves the plasma in the form of electromagnetic radiation, ions (unburned D fuel, unburned T fuel and thermalized alphas), electrons and neutrals (from charge exchange events). The plasma radiation and particle fluxes result in surface heat loads and erosion at the first wall and divertor plate.

Table 1
Maximum nuclear environmental conditions at the first wall of the ARIES-I design

Neutron wall loading	3.3 MW/m^2
Neutron flux	1.22×10^{15} n/cm^2 s
Displacement rate	36 dpa/yr
Helium production rate	5280 appm/yr
Hydrogen production rate	1450 appm/yr

Table 2
Summary of the ARIES-I SiC/SiC-composite thermo-mech. analysis

	Analysis
First Wall	
Maximum SiC/SiC temperature	940°C
Maximum SiC/SiC stress ($T + P$)	77 MPa
Divertor plate	
Maximum SiC/SiC temperature	692°C
Maximum SiC/SiC stress ($T + P$)	121 MPa

Table 3
Properties of the SiC composites used in the Aries-I design

Property	Composite [a]	CVD layer
Density (kg/m^3)	2500	3100
Young's modulus, E (GPa)		
E_x	364	320
E_y	360	320
Poisson's ratio, n	0.16	0.17
Thermal-expansion coefficient, a (10^{-6}/K)		
a_x	4.4	4.5
a_y	4.3	4.5
Thermal conductivity, k (W/K m)		
k_x	15	15
k_y	12	15
Allowable stress (MPa)		
Primary	140	140
Secondary	190	140

[a] Properties were calculated using the CLASS code (2) with a ply orientation pattern of $-45°/0°/45°/90°$, a fiber volume fraction of 60%, and a void fraction of 10%.

Table 4
Summary of major feasibility issues for application of SiC/SiC composites in ARIES-I

Issues	Comment
Hermeticity	helium coolant pressure is 10 MPa
Thermal conductivity	irradiated value of ~ 15 W/K m was adopted
Radiation stability	lifetime of 18 MW yr/m^2 was assumed
Transmutation effects	effects of He and H transmutation products not known
Thermal shock	plasma disruption can result in thermal shock issues
Fatigue	shutdown and startup issues must be considered

The first wall, blanket and divertor plate of ARIES-I employ SiC/SiC composites as structural material. The first wall/blanket/divertor plate capture over 90% of the fusion energy at high temperature and helium coolant (pressurized to 10 MPa) removes this energy as heat which eventually drives a turbine. The blanket also contains a lithium-bearing compound in which neutron interactions breed tritium which is recovered and then fed back into the plasma as fuel. Fig. 2 shows a section of the ARIES-I first wall design. Note that a 2 mm thick chemical vapor deposited (CVD) layer of SiC is proposed to provide hermeticity, i.e., the helium coolant is at a pressure of 10 MPa while the plasma pressure is negligible.

Table 1 summarizes the maximum nuclear environmental conditions at the first wall of the ARIES-I design. Table 2 summarizes the results of the thermo-mechanical analysis for the ARIES-I SiC/SiC first wall and divertor plate and Table 3 summarizes the SiC/SiC material properties used in the thermo-mechanical analysis [2]. Table 4 summarizes the major feasibility issues associated with the application of SiC/SiC composites in the ARIES-I design.

3. Material properties

3.1. Overview of SiC / SiC properties

There are potentially a number of fibers and matrixes that could lead to radiation resistant ceramic matrix composites. However, a summary of the properties of only SiC/SiC are presented because this material is the leading candidate for this application and is the material with the largest unirradiated and irradiated data base.

The properties of composite material can be tailored to fit a specific application by choice of fiber, fiber architecture, fiber/matrix interface and processing route. Therefore, handbook or published values of material properties are only valid for a specific combination. For the purpose of comparison, a summary of the properties of SiC/SiC produced by several processes and suppliers is given in Table 5. Included in this table are SiC/SiC materials produced by chemical vapor infiltration CVI by SEP in France, as reported by Fenici and Scholz [3] and DuPont[(a)] in the United States, an enhanced SiC/SiC with improved high-temperature oxidation resistance produced by CVI at DuPont[(b)] and a SiC/SiC produced at DOW[(b)] by the polymer-impregnation-pyrolysis (PIP) route. Each of these materials have a 0/90 Nicalon® fiber lay-out, 40% fiber volume fraction and a carbon interfacial layer between the fiber and matrix. The thickness of the carbon interfacial layer can have a significant impact on the material strength and fracture toughness; however, the thickness of the carbon layer for each of the data sets in Table 5 is unknown.

Comparison of the data presented in Table 5 shows that the properties of these materials are very similar with a few exceptions. The SEP and DuPont materials are very similar since they are made by the identical process. DuPont is under license to use the SEP process. Even though the data was obtained from different sources, the SEP and DuPont data appear to be the same data set for some properties except for the tensile elastic modulus, tensile fracture strength, and elongation. This difference could be the result of SEP and DuPont applying different carbon thicknesses in the fiber/matrix interface; however, both the tensile strength and elongation would not be expected to decrease simultaneously unless the carbon layer thickness is less than an optimal value. The fracture strength has been shown by Lowden [4] to decrease with increasing carbon layer thicknesses for carbon layer thickness equal to or greater than 0.2 μm.

DuPont's enhanced SiC/SiC is also produced by the CVI process and many of the properties are similar to the SEP and DuPont material. The most significant exception is the Young's modulus of the DuPont material which is about 36% less for the enhanced SiC/SiC material. The DuPont material with the newer Hi-Nicalon® fiber exhibits a higher Young's modulus and flexure strength but similar tensile properties to DuPont material with Nicalon® fibers. The enhanced material has a proprietary additive that improves its oxidation resistance at elevated temperatures. It appears that this additive caused the tensile modulus to decrease. The PIP process used by DOW/Kaiser requires multiple cycles to achieve optimum properties; although, as shown by the data in Table 5, this material can have a lower porosity than that made by the CVI process. However, the tensile modulus is about $\frac{1}{3}$ and

Table 5
Properties of several SiC/SiC composites

Property	Units	SEP		DuPont		DuPont enhanced SiC/SiC		DOW/ Kaiser S-201		DuPont Hi-Nic
		296 K	1273 K	296 K	1273 K	296 K	1273 K	296 K	1273 K	296 K
Fiber content	%	40	40	40	40	40	40	40	40	40
Specific gravity	kg m^{-3}	2500	2500	2500	2500	2300	2300	2100	–	2700
Porosity	%	10	10	10	10	10	10	4	4	–
Tensile strength	MPa	285	285	200	228	228	254	207	–	217
Elongation (tensile)	%	0.65	0.75	0.22	0.28	0.41	0.61	–	–	0.23
Young's modulus (tensile)	GPa	230	200	215	226	141	145	80	–	270
Flexural strength	MPa	300	400	300	400	345	–	366	–	336
Compressive strength										
In plane	MPa	580	400	580	480	503	–	450	–	–
Through the thickness	MPa	420	380	420	380	–	–	–	–	–
Shear strength (interlaminar)	MPa	40	35	40	35	31	–	28	–	–
Thermal diffusivity										
In plane	10^{-6} m^{-2} s^{-1}	12	5	12	5	–	–	1.1	0.7	–
Through the thickness	10^{-6} m^{-2} s^{-1}	6	2	6	2	1.5 [a]	–	0.8	0.6	8.7
Coefficient of thermal expansion										
In plane	10^{-6} K^{-1}	3	3	3	3	3	2.9	4.3	–	–
Through the thickness	10^{-6} K^{-1}	2.5	2.5	2.5	2.5	2.9	–	–	–	–
Fracture toughness	MPa $m^{1/2}$	30	30	30	30	–	–	–	–	–
Specific heat	J kg^{-1} K^{-1}	620	1200	620	1200	–	–	727	1248	–
Total emissivity		0.8	0.8	0.8	0.8	0.8	0.8	0.94	–	–

[a] Thermal conductivity (W/m K).

the thermal diffusivity about a factor of between $\frac{1}{5}$ to $\frac{1}{10}$ that of the CVI processed material.

The reason for the lower modulus and thermal diffusivity is likely related to the low pyrolyzing temperature (< 1200°C) used to minimize damage to the Nicalon® fibers. Significant crystallinity does not result from these preceramic polymers at pyrolyzing temperatures below 1400°C [5,6].

3.2. Some specific properties of continuous fiber ceramic composites

Continuous fiber ceramic composite (CFCC) properties are controlled by the fiber strength, volume fraction, weave, fiber/matrix interface and matrix properties. Metal and polymer matrix composite properties follow a rule of mixtures relationship as described by Eq. (1) where P_c, P_f and P_m are the composite, fiber and matrix property, respectively, and V_f and V_m the fiber and matrix volume fractions, respectively,

$$P_c = P_f V_f + P_m V_m. \quad (1)$$

However, CFCCs do not obey this simple relationship for many of their properties and particularly for their fracture strength. This point is demonstrated by comparison of the composite properties given in Table 5 and the Nicalon® fiber data given in Table 6 [7]. The fracture strength of Nicalon® is listed as 3.0 GPa and according to Eq. (1), the composite fracture strength should be 600 MPa for 40% volume fraction of 0/90° aligned fibers. This value is approximately a factor of three larger than the measured fracture strengths given in Table 5. The composite modulus and density are less than the modulus and density of stoichiometric SiC (3200 kg/m^3) because the polymer derived fibers have moduli and densities less than stoichiometric SiC and the SiC/SiC composites have between 4 and 10% porosity. Factors that control several specific properties for CFCCs will be discussed in the following sections. These properties were selected because they are generally needed for most high temperature applications; however, the relative importance of each of these properties is design specific. Also, other properties such as corrosion, hermetic behavior, and the behavior of joints are highly design specific and therefore, will not be discussed.

3.2.1. Thermal conductivity and diffusivity in CFCCs

Lattice vibrations (phonons) account for the majority of the heat transport in ceramics such that the lattice thermal conductivity can be described as follows:

$$K = \tfrac{1}{3} c_v v l \rho, \quad (2)$$

where c_v is the lattice specific heat at constant volume, v the phonon velocity, l the phonon mean free path and ρ is the density. Ceramics exhibit a maximum thermal conductivity at low temperatures with a decreasing conductivity with increasing temperature. The maximum thermal conductivity is a function of lattice defects, interfaces, and impurities. The temperature dependence of the thermal conductivity for SiC made by chemical vapor deposition (CVD), SiC/SiC composites made by CVI (in-plane values) and Nicalon® fibers is given in Fig. 3. It is apparent from these data that Nicalon® fibers contribute very little to the conductivity of the composite but result in a reduction in the composite relative to SiC because they effectively reduce the thermal transport area. These data are consistent with Eq. (1) where a simple rule of mixtures is

Table 6
Properties of as-produced silicon-based fibers (DiCarlo [7])

Process	Composition	Tradename	Diameter	Average strength (GPa)	Modulus (GPa)	Density (g/cm^3)	Expansion coefficient [a] (ppm/°C)
CVD	SiC on W	SIGMA	100	3.5	410	3.4	
		C-1	127	3.4	412	3.2	4.8
	SiC on C	SC5-6	142	4.0	390	3.0	4.6
		SC5-9	75	3.5	365	2.9	
		[TEX]	50/142	[5.0]	320/410	2.8/3.0	
Polymer pyrolysis	Si–C–O	Nicalon®	14	3.0	220	2.55	
		Hi-Nicalon®	14	2.8	270	2.74	
		near stoichiometric Hi-Nicalon	14	3.0	400–460		
		Tyranno	10	3.0	190	2.4	3.1
	Si–N–C–O	Tonen	10	2.5	250	2.5	
		HPZ	10	3.0	245	2.4	
		Fiberamic	15	1.8	220	2.4	3.1
Sinter	SiC	[D–C]	10	[3.5]	420	3.1	4.6
		[CAR]	[30]	[1.5]	420	3.1	4.6
Chemical conversion	SiC	[MER]	5	[]	340–410	2.9–3.1	4.6

[a] Average from 20–1000°C.

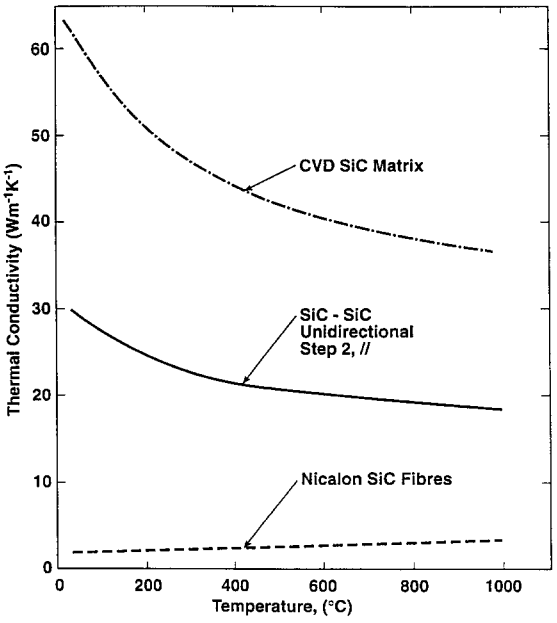

Fig. 3. Thermal conductivity of a SiC/SiC composite, Nicalon® fibers and CVD SiC as a function of temperature.

adequate to describe the thermal conductivity of the composite material.

Thermal diffusivities for several SiC/SiC composites are given in Table 5. Only thermal conductivity data is available for the enhanced SiC/SiC produced by DuPont. There is a factor of 2 to 2.5 difference between the in-plane and through thickness diffusivity values that reflects the greater amount of scattering from porosity, fiber/matrix interfaces and growth interfaces in the CVI matrix. Also, the DOW/Kaiser material has between a factor of 5 to 10 lower thermal diffusivity than the CVI produced materials. In fact, the thermal properties of the DOW/Kaiser material are more consistent with that of the fibers than β-SiC because of its amorphous (noncrystalline) structure.

Thermal conductivity (K) is a function of thermal diffusivity as described by

$$K = \rho \alpha_d C_p, \tag{3}$$

where ρ is the material density, α_d is the thermal diffusivity and C_p is the material heat capacity. However, a comparison between the thermal diffusivities of the materials listed in Table 5 is not possible because the heat capacity of the enhanced SiC/SiC has not been reported. However, the proprietary additive is unlikely to affect the heat capacity of the enhanced SiC/SiC.

3.2.2. Fracture strength and toughness

Continuous fiber reinforced composites acquire their strength and toughness from the presence of the continuous fibers, but each property results from a different mechanism. The nature of the fiber/matrix interface is a key factor in attaining the optimum fracture strength and fracture toughness. The mechanisms controlling fracture strength, fracture toughness and crack growth processes in CFCCs have been described in a number of publications including Evans and McMeeking [8], Marshall et al. [9] and Evans [10].

A comparison of the stress–strain response of CFCCs and monolithic ceramics, as shown in Fig. 4a and b, respectively, illustrates the contribution of the continuous fibers to their strength. The fracture toughness is proportional to the work of fracture or the area under the stress–strain curve so the improved fracture toughness is also illustrated by Fig. 4a. The schematic shown in Fig. 4a illustrates the key features of the stress–strain response of CFCCs including the matrix cracking stress, fiber bundle failure stress and the effect of fiber pull-out on strain to failure. These processes produce a nonlinear stress–strain response that increases the total failure energy. This is in contrast to the stress–strain response for monolithic ceramics shown in Fig. 4b, where the stress–strain response is linear-elastic up to the fracture stress after which unstable flaw growth occurs.

Important features of the stress–strain response of CFCCs include: (1) matrix cracking stress, (2) the maximum fracture strength and (3) strain to failure. The matrix cracking stress is a function of the fiber strength and the fiber/matrix interfacial strength. The stress–strain response of CFCCs approaches that of monolithic material with increasing fiber/matrix interface strength so that the matrix cracking stress becomes the failure stress at very high interfacial strengths. Clearly, the matrix cracking stress increases with increasing fiber strength while an increase in the fiber/matrix interfacial strength can cause a decrease of the fracture toughness.

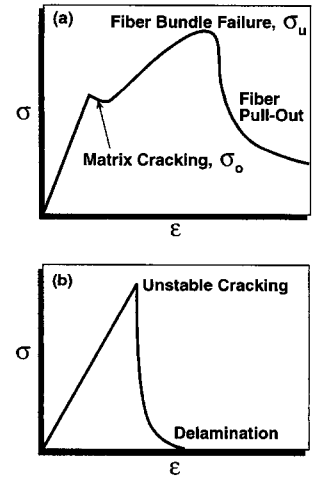

Fig. 4. Schematic illustrating the range of stress–strain characteristics exhibited by (a) ceramic matrix composites and (b) monolithic ceramics.

Specific details of fiber/matrix debonding ahead of the crack, in the wake of the crack, the fiber/matrix sliding stress and fiber pull-out and fracture toughness of CFCCs have been previously detailed by [8–10]. The schematic given in Fig. 5 illustrates the critical processes controlling the toughness of CFCCs. Critical parameters controlling the toughness are identified by Evans [10]: (1) the relative fiber/matrix interface debond toughness, (2) the thermal expansion misfit strain between fiber and matrix, (3) the coefficient of friction between the fiber and matrix, (4) the fiber strength, (5) the fiber strength distribution or Weibull modulus, m, (6) the matrix toughness and (7) the fiber volume fraction. Large fiber pull-out results from high strength fibers with a small m and a small fiber/matrix coefficient of friction.

Fiber/matrix debonding is a critical step in the behavior of these materials. During matrix crack growth, debonding occurs initially at the crack front, with crack advance through the matrix followed by further debonding in the crack wake. The extent of crack wake debonding is a function of the magnitude of the residual radial stress. Large residual radial tensile stress and smooth fibers result in large debonding while residual radial compressive stress and a rough fiber surface reduce the extent of debonding. The extent of fiber pull-out in the wake of the crack is then determined by the Weibull modulus and the coefficient of friction between the fiber and matrix. A high Weibull modulus and a high coefficient of friction reduce the extent of pull-out. Conversely, a low Weibull modulus and a low coefficient of friction increases the extent of fiber pull-out. The energy required to extend the crack and, ultimately, the fracture toughness is a complex function of the debond length and interfacial stress with the optimum toughness corresponding to intermediate values of pull-out length and interfacial stress.

For the data given in Table 5, the tensile strength corresponds closer to the maximum fracture strength in Fig. 4 then the matrix cracking strength. The matrix cracking strength is generally about $\frac{1}{3}$ to $\frac{1}{2}$ that of the ultimate strength so it ranges between 100 and 200 MPa for these materials depending on loading mode. The ultimate strength is associated with fiber bundle failure and is therefore closely coupled to the fiber strength. The tensile strengths are very similar, since these materials have the same volume fraction of Nicalon® fibers. The difference in the elastic modulus of the DuPont enhanced SiC/SiC and DOW/Kaiser PIP SiC/SiC primarily reflects the difference in the matrix composition and structure of these composites relative to the CVI material. The variation in tensile elongation reflects differences in fiber debonding, pull-out and the energy to extend a crack through the matrix in the presence of the SiC fibers. There are likely differences in the interface debond strength, residual radial stresses and fiber/matrix coefficient of friction for these materials because of their differences in composition, structure and matrix processing methods.

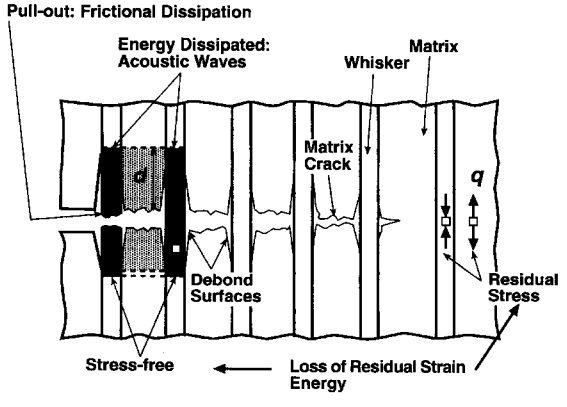

Fig. 5. Schematic illustrating the various energy absorbing contributions to the steady state toughness.

3.2.3. Creep and time dependent crack growth of CFCCs

High-temperature properties are one of the primary advantages of structural ceramics relative to metallic or intermetallic materials. Therefore, their high-temperature creep and time dependent crack growth properties could define maximum use temperatures or stresses. Creep of whisker-reinforced ceramics has been studied extensively and this field was recently reviewed by Wiederhorn and Hockey [11]. However, there is much less information available on creep of CFCCs. Holmes and Chermant [12] recently reviewed the status of creep behavior of CFCCs and concluded that the microstructural damage that occurs during creep is a function of the relative creep rates of the fibers and matrix. For the case where the fiber/matrix creep rate (FMCR) ratio is less than unity, microstructural damage involves debonding of the fiber/matrix interface followed by periodic fiber fracture. When the FMCR ratio is greater than unity, matrix fracture and fibers bridging the cracks is the crack growth mode. Holmes and Chermant concluded that the first case where occasional fiber fracture occurs without matrix cracking is less damaging than the second case where fiber bridged matrix cracking occurs. The second case is considered worse than the first because the matrix cracks will expose the fibers to the environment and the entire load must then be supported by the bridging fibers. The exposure of the fibers to the environment because of matrix cracks, is clearly a concern for applications in corrosive environments. However, it has been demonstrated by Henager and Jones [13] that for SiC/SiC composites the Nicalon® fibers are the primary load bearing component in the composite so that when the fiber creep rate exceeds the matrix creep rate, it can be beneficial in the absence of oxidation.

An example of the beneficial effect of fiber creep during matrix crack growth is shown in Fig. 6 for a 0/90 SiC/SiC composite with Nicalon® fibers and a CVI SiC

matrix tested at 1100°C in argon [14]. When the original cross-section is used to calculate the fracture strength, the material strength decreases with increasing depth of a machined notch. However, when cracks of similar length are produced by high-temperature subcritical crack growth and the original cross-section is used to calculate the fracture strength, there is no effect on strength with increasing matrix crack depth. This insensitivity to matrix cracking results from stress relaxation in the bridging fibers and the resulting increase in bridging length. Without creep, the fibers farthest from the crack tip would fracture resulting in a fracture strength less than material without a crack. Likewise, in samples with machined notches, fibers do not bridge the crack so that the composite strength is decreased with increasing notch depth. Conversely, samples with cracks produced by subcritical crack growth under conditions of fiber creep essentially have all the bridging fibers intact so the fracture strength is insensitive to crack length. These results suggest that it may be more desirable to maintain the fiber integrity, as in the case where the FMCR ratio is greater than unity. Matrix cracking is clearly a concern when there is a corrosive or oxidizing environment; however, matrix microcracking may be unavoidable in CFCCs especially at stress concentration, or as a result of thermal or stress cycles.

The presence of matrix cracks will produce a condition where subcritical crack growth can occur. This type of behavior has been evaluated by Henager and Jones [13] for SiC/SiC composites. Their results show that the crack velocity versus applied stress intensity (SCG curves) for SiC/SiC has a stage II region where the crack velocity is essentially independent of the applied stress intensity, followed by a stage III, or power-law, crack-growth region at high stress intensities, Fig. 7. The power-law region exhibits a strong dependence on applied stress intensity, but the stage II region only a weak dependence. The SCG data for monolithic ceramics that do not exhibit a large-scale bridging zone do not show stage II behavior; rather, crack

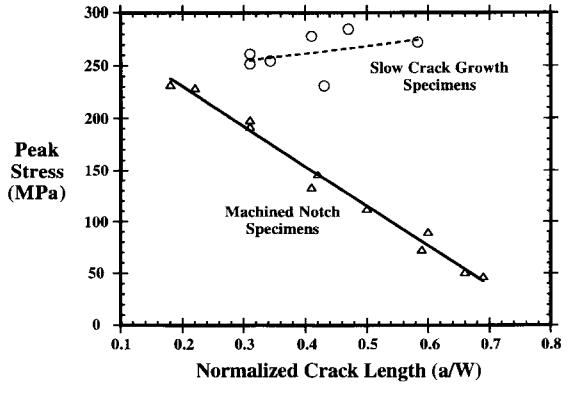

Fig. 6. Peak stress at 1100°C for SiC/SiC samples with cracks introduced by subcritical crack growth at 1100°C and machined notices.

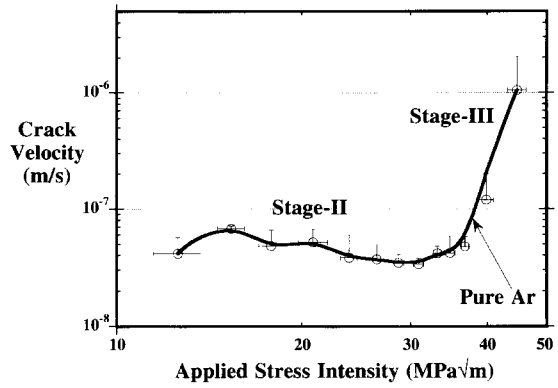

Fig. 7. Subcritical crack growth velocity for a SiC/SiC composite at 1100°C in a high purity Ar environment.

velocity is a power-law function of applied stress intensity (K_A) [15–18]. The stage II region in the present data reveals a weak dependence on K_A, suggesting that SCG in CFCCs is controlled by crack bridging by the continuous fibers in the crack wake. The bridging zone screens, or shields, the crack-tip from the applied stress intensity. Over the region where K_A increases as a function of increasing crack length, a bridging zone is established for these materials, and it screens the crack tip from K_A. A nearly constant crack tip stress intensity, K_{tip}, is established as the bridging zone develops and R-curve behavior is observed. Eventually, the bridging zone saturates and cannot continue to increase the crack-tip shielding. The stage II crack velocity is thermally activated with an activation energy of 234 ± 50 kJ/mol over the temperature range of 800 to 1100°C. Modeling and analysis can explain the stage II behavior by creep of the bridging fibers, which reduces the closure force applied by these fibers and hence decreases shielding of the crack tip from the applied stress intensity. Hence, the crack velocity increases with increasing temperature.

3.2.4. Cyclic load (fatigue) behavior of CFCCs

There have been relatively few studies of the fatigue behavior of CMCs, and most of these have been conducted at high frequencies. Several factors affect the performance of composite materials in cyclic stress applications, for example: (1) compressive stress can cause delamination and microbuckling [19] and (2) tension–tension tests conducted at stresses below the matrix-cracking stress cause little fatigue damage [20]. A regime where fiber interface sliding occurs has also been identified by Rouby and Reynaud [21] as causing fatigue damage in tests on 1D SiC/SiC tested at a frequency of 1 Hz and room temperature. Rouby and Reynaud observed an endurance limit at which failure did not occur after 250 000 cycles and a regime where fatigue damage and failure occurred after 5 to 12 000 cycles. The endurance limit observed by Rouby and Reynaud exceeded the matrix-cracking stress by about

30% in contrast to the results of Holmes who observed an endurance limit equal to the matrix-cracking stress.

Results of low cycle fatigue tests conducted on SiC/SiC at 1100°C in a high-purity Ar environment [22] are shown in Fig. 8. This test was conducted at a R value of 0.1 and with 1000 s hold time at load and 25 cycles at each stress intensity value. Crack velocity decreased with increasing number of load cycles at low stress intensity, as demonstrated by the crack velocities after the first and 25th load cycle. This effect was diminished at high stress intensities. The decrease in crack velocity at low stress intensities is understood from observations of decreasing crack velocity as a function of hold time at constant load. This effect results from creep relaxation of the bridging fibers and the resulting increase in the number of fibers bridging the crack. The convergence of the two curves in Fig. 8 at high stress intensity results either from fatigue damage with increasing number of cycles or from the fracture of bridging fibers that occurs for either constant or cyclic loads with increasing stress intensities. The crack velocity for the cyclically-loaded specimen is less than that for a statically-loaded specimen over the entire stage II region. Therefore, it would appear that there was no fatigue damage for this test. Rouby and Reynaud [21] noted that fatigue failure was commensurate with a decrease in the tangential Young's modulus during high-cycle fatigue in 2D SiC/SiC composites. In the present test, the elastic modulus decreased by 20% between the first and last cycle. However, some decrease in modulus is expected as the stress intensity approaches stage III because of fracture of the bridging fibers. More testing, conducted under constant K conditions, is required to determine the conditions that induce low-cycle fatigue damage of SiC/SiC at elevated temperatures.

Holmes et al. [23] measured the cyclic creep or low cycle fatigue behavior of SiC fiber reinforced Si_3N_4 at 1200°C for several cycles of creep and recovery times. They found that there were fewer fiber failures when there

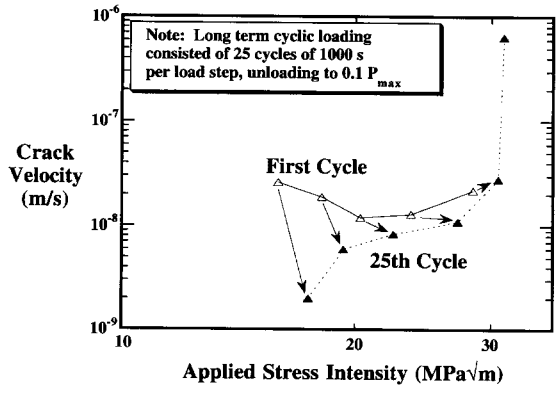

Fig. 8. Low cycle fatigue behavior for a SiC/SiC composite at 1100°C.

was a recovery cycle (i.e., the load reduced to $0.01P_{max}$) as compared to either static load or cycling without any hold time during the unloaded period. For instance, there were 10% fiber failures for samples loaded 300 s and unloaded 300 s, 30% fiber failures for samples loaded 50 h and unloaded 50 h and 40% fiber failures for sustained loads. They attributed the reduced number of fiber failures to the reduction in fiber stress that occurs during the recovery period. The results of Holmes et al. are similar to those of Jones and Henager [22] where the crack growth rates decreased with increasing number of cycles at a given stress intensity. The creep relaxation of the fibers with time and the greater amount of time associated with increasing number of cycles contributed to this decrease.

3.2.5. Thermal shock behavior of CFCCs

Thermal shock behavior of CMCs is highly dependent on the temperature change (ΔT) occurring during rapid energy deposition from the plasma during a disruption. This ΔT effect was demonstrated in a study of the thermal shock behavior of SiC whisker reinforced Al_2O_3 reported by Lee and Case [24]. They measured the modulus and internal friction as a function of thermal shock cycles and found that: (1) saturation in the damage level was dependent on ΔT^6, and (2) damage saturated after 49 cycles at a ΔT of 270°C and after three cycles for a ΔT of 380°C. Kagawa et al. [25] found that thermal shock behavior of SiC fiber reinforced glass was better than that of unreinforced glass. Elastic modulus and fracture strength after a single quench from variable temperatures showed no evidence of damage in the composite below 373°C while the unreinforced glass showed damage above 273°C.

Thermal shock tests on SiC/SiC composites have been reported by Eckel et al. [26] at the NASA/Lewis Research Center and by Wang and Singh [27]. The NASA tests were conducted in a H_2–O_2 burner rig with ΔT ranging from 1300 to 2300°C. The thermal shock was created by rapid heating in contrast to other reported thermal shock tests where thermal shock was created by rapid cooling. Monolithic SiC failed in 1.5 cycles at a heating rate of 1400°C/s while the SiC/SiC composite withstood 25 cycles with a 1700°C/s heating rate with little or no decrease in the tensile strength. A 35% strength loss was noted after 25 cycles with a 1900°C/s heating rate, but this effect was related to erosion and not composite cracking. Thermal shock results from the CFCC made with DOW/Kaiser Ceramic Composites PIP process are presented in Fig. 9 [27]. Since cycle thermal shock tests were conducted by heating a bend bar to a specified temperature up to a maximum of 1000°C, followed by quenching in water. A reduction in strength was observed for temperatures greater than 400°C with some recovery of this loss above 800°C. The maximum loss of strength was 29%. Comparison between the NASA burner rig test and the DOW/Kaiser quench test indicates that thermal shock produced by rapid

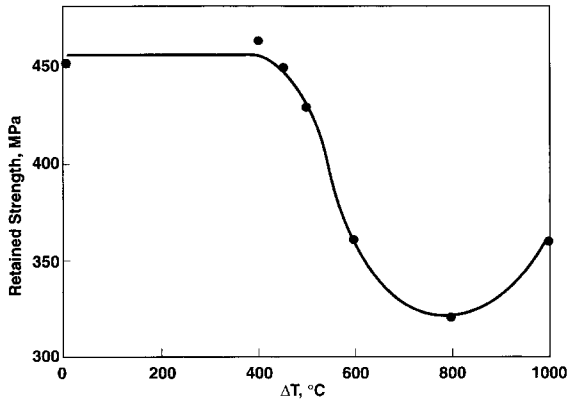

Fig. 9. Thermal shock behavior for a SiC/SiC composite made by the Kaiser Ceramic Composites polymer-impregnation-pyrolysis process.

quenching is more severe than by rapid heating. Therefore, a relevant thermal shock test must simulate the conditions expected for a specific application.

4. Radiation stability of SiC/SiC composites

4.1. Fundamental aspects of radiation damage in SiC

Displacement damage caused by incident radiation results in the formation of lattice defects that can change the microstructure and properties of the material. Understanding the nature of defect production at the atomic scale, the 'primary damage state', underpins the science of radiation effects. There are two immediate objectives in studying the primary damage state in SiC: to understand the mechanisms of the production and evolution of defects and their roles in microstructural changes, and to quantify the damage in terms of displacements of atoms in radiation events for the purpose of correlating and extrapolating experimental results under different irradiation conditions.

Considerable progress has been made in understanding the fundamentals of radiation damage in SiC and a few other ceramic materials, but many of the important details remain unknown. Although much more is known about radiation damage at the atomic scale in metals than in ceramics, much of what has been learned in metals forms a template for the investigations required for SiC and other less-studied materials.

The primary damage state is investigated by experiments and computer simulations. Many radiation damage experiments measure the effects of irradiation over time and distance scales that are too large to give direct information on the primary damage state of a cascade and the details of its formation. Computer simulations can be used to investigate the production and evolution of defects at time and distance scales inaccessible to experiments. Aspects of the primary damage state in SiC that, in principle, can be directly addressed in experimental measurements and used to validate simulations include displacement threshold energies, defect properties such as formation and migration energies, and amorphization.

4.1.1. Computer simulations

Computer simulation methods consist of several major types, including the most realistic 'first principles' calculations that can deal with tens (or perhaps hundreds) of atoms, molecular dynamics (MD) using many-body pair potentials that can deal with up to millions of atoms on massively parallel computers, binary collision calculations that predict the overall size and shape of cascades up to the highest cascade energies, and stochastic annealing simulations that treat lattice defects as the interacting entities. All of these simulation methods depend on using realistic models for atomic interactions. This issue is particularly important in MD calculations, where a wide variety of interatomic potential models has been put forth. Many-body interatomic potentials developed for SiC can be classified as one of the following types: (1) potentials developed following the Born–Oppenheimer expansion, (2) potentials modeling the local atomic environment using electron distributions and (3) potentials introducing local environment effects into pair potentials. These three categories are represented by the Pearson potential [28] the modified embedded atom method (MEAM) [29] and the Tersoff potential [30], respectively.

4.1.2. DPA calculations

The displacement threshold energy is the energy required to remove an atom from its lattice site and create a stable vacancy–interstitial (Frenkel) pair. Comparison of experimental and theoretical displacement threshold energies is perhaps the best measure of the validity of displacement cascade simulations (assuming, of course, that the interatomic potential used in the simulation model also predicts well other measurable quantities-elastic constants, vacancy formation energy, etc.). The displacement threshold energy is also used in calculating the 'displacements per atom' (DPA), a calculated exposure or dose parameter that allows the comparison of radiation damage of a material irradiated in different sources, e.g., different neutron spectra or ion beams. DPA, which is a calculated measure of the potential for creating damage, not only accounts for the fluence of incident radiation, but also provides a measure of the response of the material to the radiation. (Note that the calculated DPA value is not a measure of accumulated residual damage; the actual number of defects produced in a given irradiation is much less than the number of calculated displacements.)

The calculation of DPA requires a knowledge of the electronic and nuclear stopping powers of ions in the material as well as the displacement energy. From this

information a displacement function is obtained that is integrated over the energy spectrum of the recoil atoms produced by the incident radiation. In polyatomic materials, the displacement function is typically calculated either by the numerical solution of coupled integro-differential equations defined by Parkin and Coulter [31–33] or by using the Monte Carlo ion transport computer code TRIM [34]. The former is commonly used for neutron irradiations and the latter for ion-beam irradiations. Recently, Weber et al. [35] compared the two methods of calculating displacements for SiC, pointing out the importance of using a consistent model for electronic stopping power in all calculations.

4.1.3. Threshold energy experiments

Perhaps the most uncertain part of DPA calculations for SiC is the value of the displacement energy. In monatomic metals, for which the concept of DPA was originally devised, the displacement threshold energy can be determined experimentally by resistivity measurements. In SiC a number of phenomena have been tried as quantitative indicators of defect formation, including resistivity, luminescence, positron annihilation, amorphization, and defect cluster formation, but consistent values of displacement threshold energies have not been obtained among these methods. No technique measures defect concentrations directly, only be inference, and each technique is subject to limitations on such variables as minimum detectable defect concentration, temperature, impurities or existing microstructure. The difficulty sometimes lies in knowing the relationship between the measured quantity and the production of defects. The problem is further complicated, of course, by the fact that two species of atoms can be displaced, and they may have significantly different displacement energies, hence, they may exist in different relative concentrations. The displacement energies are also directionally anisotropic, i.e., the energy required to form a stable defect pair depends on the direction the atom is ejected from its original site. Since carbon atoms are the easiest to displace, the displacement threshold energy for carbon atoms is the easiest to measure. A recent survey of displacement threshold energy measurements for SiC by Zinkle and Kinoshita [36] indicates a range of 20–25 eV measured for carbon atoms, while those for silicon atoms range from 20–50 eV. The authors of the survey recommended values of 20 eV for carbon and 30 eV for silicon, noting the large uncertainty for silicon.

4.1.4. Calculated displacement energies

Calculated values of the displacement energy from molecular dynamics (MD) simulations have been equally as inconsistent as the experimental values, because of the difference in interatomic potentials used for SiC. El-Azab and Ghoniem [37] obtained directionally averaged values of 93 eV for Si and 16 eV for C using a Pearson potential. Values by Wong et al. [38], using a Tersoff potential were 45 eV for Si and 35 eV for C, when similarly averaged (minimum values were 35 eV and 25 eV for Si and C, respectively). In a subsequent calculation of defect energetics in SiC, Huang et al. [39], compared three many-body interatomic potentials (Pearson, Tersoff and the MEAM). The Pearson potential used for displacement calculations in Ref. [37] was shown to be clearly inferior to the other many-body potentials considered when compared with values of defect migration and formation calculated by first principles methods. The other two potentials were about the same, with the Tersoff potential doing slightly better overall. On the basis of those results, the displacement energy calculations of Ref. [37] should probably be rejected.

A standard set of realistic displacement energy values universally used to calculate DPA in SiC does not presently exist. A standard should be determined and agreed to, so the growing body of data from irradiation experiments can be compared consistently. Perhaps MD simulations may provide the best values of displacement energies to use, if a specific set of interatomic potentials that are well-validated against many physical properties of SiC and reproduce the carbon displacement energy of about 20 eV can be developed.

4.1.5. Displacement damage cross-sections

Once a standard DPA damage model is established for SiC, displacement damage cross-sections as a function of neutron energy can be calculated and used to determine DPA levels for irradiations in any neutron spectrum. Cross-sections have been determined by Huang and Ghoniem [40], but they are based on displacement energies that were generated with the Pearson potential, which predicts that nearly all the damage is in the form of carbon atom displacements. Nevertheless, a general conclusion can be drawn from these cross-sections that the neutron energy dependence of the displacement cross-sections for SiC is significantly different from that of stainless steel. The cross-sections indicate a higher DPA rate in SiC than in stainless steel for neutron energies in the range 0.1 MeV $< E <$ 1.0 MeV, but a lower DPA rate for SiC relative to stainless steel for neutrons with $E >$ 1.0 MeV.

4.1.6. Defect properties

Based on MD simulations using the MEAM, the activation energy of silicon self-diffusion (thermal diffusion through a vacancy mechanism) is 10.7 eV, while that of carbon is 8.3 eV. These results are in good agreement with experimental data [41,42], which are 9.50 and 8.70 eV for silicon and copper, respectively. The values obtained with the Tersoff potential are 11.86 and 14.12 eV, respectively.

Computer simulations of defect energetics in SiC indicate that the large difference in atomic 'size' between carbon and silicon dictates much of the migration behavior [39]. It is found that while the energy for direct migration of a silicon vacancy is reasonably consistent with experi-

mental observations (above 2.9 eV for the MEAM), the corresponding value for a carbon vacancy is higher (5.2 eV). However, once a silicon vacancy migrates, less perfect atomic configurations would exist, and carbon vacancies can actually follow at a migration energy of 2.6 eV. This argument may explain the effects of temperature on volumetric swelling, where void formation in SiC does not occur at temperatures below approximately 1000°C. Self-interstitial atoms may occupy either T-sites (tetragonal) or H-sites (hexagonal). However, interstitials at T-sites are found to be more likely to occupy a T–C site rather than a T–Si site, because more space is available at T–C sites. Interstitial atom migration appears to occur directly from one T-site to another.

4.1.7. Amorphization

At low temperature, SiC readily becomes amorphous under irradiation at temperatures below about 500 K. Determining the dependence of amorphization on temperature and the mass and energy of irradiating particles can provide a rich source of information on defect production and defect properties, especially in conjunction with results of computer simulations. A comparison of irradiations by electrons [43] and Xe^+ ions [44] demonstrates possible significant differences in amorphization. Comparing on the basis of DPA (using 25 eV as the displacement energy for both Si and C), both 2 MeV electrons and 1.5 MeV Xe^+ ion irradiations result in amorphization at doses of 0.5–0.7 DPA at temperatures less than about 250 K. However, the critical temperature above which amorphization does not occur is about 300 K for the electron irradiation and 500 K for the ion irradiation. The difference in critical temperatures may be due to the greater ease of recovery of the damage from electrons, which has a higher fraction of isolated Frenkel pairs than the ions, which produce more defects in cascades (the effects of damage rate were not considered in this comparison). The critical temperature below which amorphization occurs under neutron irradiation is reported to be less than 200 K [45].

4.2. Radiation damage in SiC / SiC composites

There is a limited amount of data on radiation effects on SiC fibers and SiC/SiC composites and it is mostly in papers by Hollenberg et al. [46], Osborne et al. [47], Snead et al. [48] and Hasegawa et al. [49]. The results presented in the following sections are a summary of these published results and some recent results obtained at the Pacific Northwest National Laboratory (PNNL) for the fusion energy systems materials program.

4.2.1. Radiation damage in fibers

The fiber is the primary load-bearing element in continuous fiber ceramic matrix composites. Therefore, the response of fibers to irradiation is critical to the response of the composite.

Table 7
Density of irradiated fibers, % change

Fiber type	430°C	800°C
Nicalon® CG	+5.3	+4.9
Nicalon® HVR	+16.5	–
Tyranno	+16.6	–
HPZ	+23.9	+4.8
DOW/NASA crystalline	+1.5	–

Density changes for fibers irradiated in FFTF at 430°C to 26 dpa (2×10^{22} n/cm^2, $E > 0.1$ MeV) is presented in Table 7. These data were obtained using the same technique as that described by Hollenberg et al. [46]. The polymer derived fibers Nicalon®, Tyranno and HPZ all exhibit significant increases in density, or shrinkage in volume, while the DOW/NASA crystalline fiber had only a 1.5% increase in density. Also shown in Table 7 is data for Nicalon®-CG (ceramic grade) and HPZ from Ref. [46] where the density change for Nicalon® is relatively independent of temperature while HPZ exhibited greater shrinkage at 430°C than 800°C. Changes that can account for these density increases include: (1) relaxation of the amorphous structure, (2) crystallization, or (3) loss of oxygen. Loss of oxygen could accompany either relaxation or crystallization.

Osborne et al. [47] evaluated the radiation response of a low oxygen Nicalon® fiber following low doses around 100°C. They reported a decrease in crystallinity from 97.5% in the unirradiated condition to 93.6% with 0.32 dpa. Fiber density was not observed to change significantly, although the data might indicate a slight decrease in density with irradiation. They also reported an increase in the tensile strength from about 2.4 GPa in the unirradiated condition to about 2.8 GPa at 0.32 dpa with a decrease in strength at lower doses. The strength increase was correlated with the crystal size; however, the cause of the decrease in crystal size with dose and the relationship to strength, was not identified.

Snead et al. [48] have summarized the effects of irradiation on SiC-based fibers and have observed that irradiation induces an increase in density in Nicalon®-CG as observed by Hollenberg et al. [46]. They also observed an increase in Young's modulus and concluded that these changes were due to recrystallization or crystal growth. Crystal growth was observed by Hasegawa et al. [49] for Nicalon®-CG irradiated with fast neutrons at 1040°C to a dose of 3.4×10^{22} n/cm^2, (43 dpa, $E > 0.1$ MeV, 185 EFPD). The crystal size was observed to change from less than 1 nm to about 5 nm as a result of this irradiation, as shown in Fig. 10. The diffraction pattern of the unirradiated materials was a series of diffuse concentric rings consistent with a material with an amorphous like structure or very fine grain size while the diffraction rings were less diffuse in the irradiated material consistent with increased ordering or crystal growth.

Hi-Nicalon®, in contrast, had a crystal size of about 5 nm prior to irradiation with little change in the crystal size following irradiation at 1040°C to 43 dpa. The greater dimensional stability of Hi-Nicalon® relative to Nicalon®-CG is very consistent with the crystal size stability.

4.2.2. Radiation damage in SiC / SiC composites

The dimensional stability of composites made from Nicalon® fibers and β-SiC matrix produced by chemical vapor infiltration (CVI) are very similar to monolithic material as shown in Fig. 11. Data are shown for composites with 150 and 1000 nm carbon interfaces, monolithic material from the same irradiation and monolithic material solid curves reported by Palentine [50,51] and Price [52]. It is apparent that the composite response is generally consistent with the β-SiC monolithic materials, but not with the Nicalon® fiber results. The 2D material with a 150 nm interphase thickness irradiated at 1200°C is inconsistent with the solid curve. The reason for this inconsistency is unknown. The Nicalon® fibers had an increase in density, or a shrinkage, on the order of 5% at both 430°C and 800°C and 26 dpa while the composite materials with Nicalon® fibers had a length change of 0.4% in the 400°C range and 0.2% at 800°C. The composite results reflect the swelling behavior of the β-SiC matrix because the fibers and matrix behave independently due to the shrinkage of the Nicalon® fibers separating them from the matrix. The monolithic SiC and the composite with the 1000 nm carbon interface exhibited similar dimensional stability to that reported by Price [52] at 1200°C but the dimensional stability of the composite with the 150 nm carbon interface was substantially better than those materials. The reason for this difference is not known.

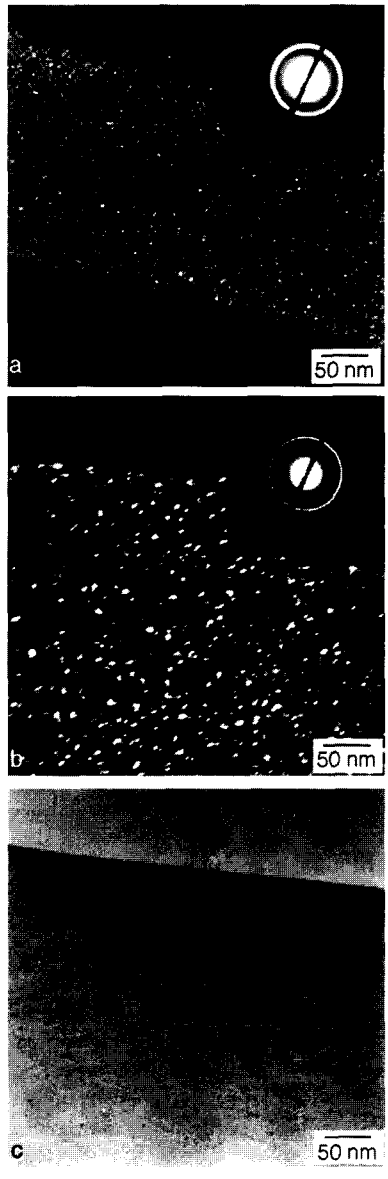

Fig. 10. Transmission electron micrographs for Nicalon®-CG irradiated at 1040°C to a dose of 43 dpa; (a) dark field for unirradiated material aged for 6000 h in Ar, (b) dark field for irradiated material, and (c) bright field image of irradiated material.

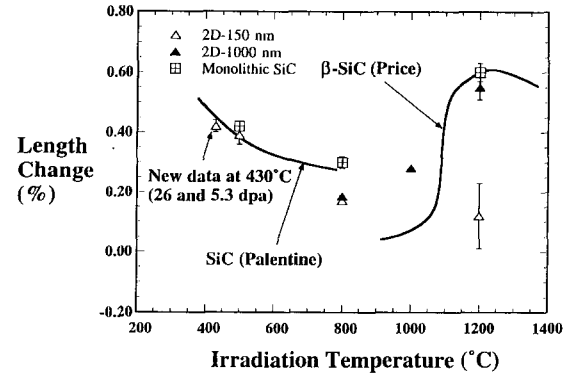

Fig. 11. Dimensional stability of monolithic beta-SiC and SiC/SiC composites as a function of irradiation temperature.

Many applications of SiC/SiC require sufficient thermal conductivity to contribute to thermal transport and to minimize thermal stresses. Therefore, the thermal conductivity of irradiated SiC/SiC is a critical property. Thermal conductivity results for SiC/SiC with the 150 nm carbon interface, as reported by Hollenberg et al. [46], are given in Fig. 12 for material irradiated at 500, 800 and 1200°C. The through thickness thermal conductivity of the unirradiated SiC/SiC was about 9 W/m K at room temperature and decreases to about 6 W/m K at 1200°C. The solid lines in Fig. 12 show the thermal conductivity upon heating following irradiation at the temperatures given on the figure while the dashed lines are for the thermal conductivity upon cooling after heating to 1200 to 1300°C. Thermal

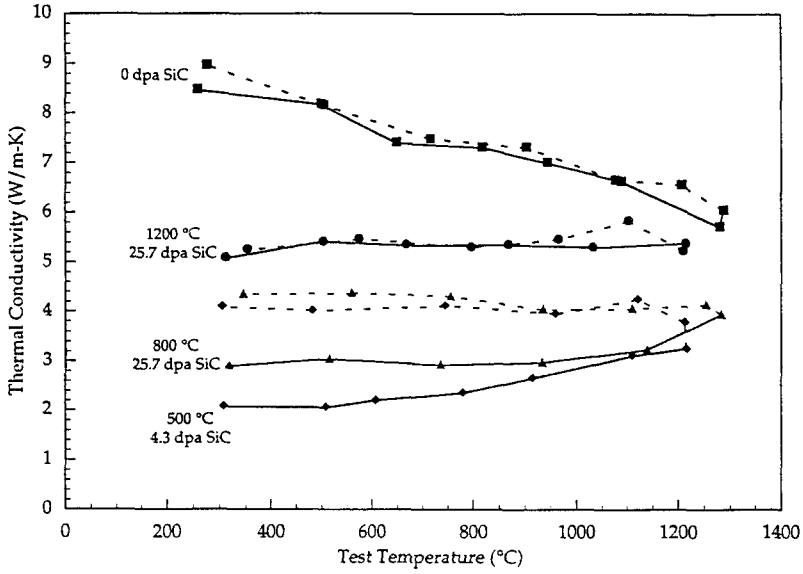

Fig. 12. Thermal conductivity of unirradiated and irradiated SiC/SiC versus temperature. Irradiations were performed at 500, 800 and 1200°C.

transport in SiC occurs by phonons and thermal resistance results from phonon scattering. Increased temperatures result in more phonon scattering and, therefore, reduced conductivity. Some of the radiation induced loss in thermal conductivity was recovered by heating to 1200°C, but residual effect remained. Heating to 1200°C annealed out some of the radiation induced scattering centers (note the lack of recovery for the material irradiated at 1200°C) but residual thermal conductivity loss persisted and the temperature dependence was unchanged. Hollenberg et al. [46] explained the residual thermal conductivity loss to vacancy clusters or voids that occur during irradiation or annealing of irradiated material at 1200°C.

Radiation effects on the thermal conductivity of monolithic SiC has been reported by Rohde [53]. Rohde irradiated polycrystalline SiC with a 6H polytype structure produced by hiping and cubic SiC produced by chemical vapor deposition. These materials were irradiated with alpha particles at 427°C with the KfK cyclotron, high energy neutrons at 327°C in LAMPF and thermal energy neutrons at 83°C in the German reactor Geestacht. The thermal conductivity of both materials was reduced from over 100 W/m K at 25°C to about 40 W/m K for the alpha particle irradiations and to about 5 W/m K for the thermal energy neutron irradiations. Partial recovery of the thermal conductivity was achieved by heating to 1420°C with greater recovery for the samples irradiated with alpha particles than those irradiated with thermal energy neutrons. Recovery of the thermal conductivity for the neutron irradiated monolithic materials was similar to the extent of recovery observed by Hollenberg et al. [46] for fast neutron irradiated SiC/SiC composites. However, in both studies a residual thermal conductivity loss persisted following annealing to 1420°C for the monolithic material and 1300°C for the SiC/SiC composite. Lee et al. [54] also measured the effects of irradiation on the thermal properties of polycrystalline alpha phase SiC. Irradiations were performed in the high flux beam reactor at Brookhaven National Laboratory at a temperature of 140°C to a fluence of 7.6×10^{20} n/cm^2. Lee et al. [54] reported a significant decrease in the thermal diffusivity at 25°C following irradiation with this decrease a factor of three between the unirradiated and irradiated material at 900°C. Thermal annealing at 1200°C resulted in some recovery but the difference in thermal diffusivity at 900°C was about a factor of two.

The four-point bend strength of irradiated SiC/SiC was found to be a function of the thickness of the interfacial carbon layer [46] as shown Fig. 13. These curves are the result of only a few specimens per condition as the irradiation volume was limited. However, the results for 19 and 26 dpa are sufficiently similar that a large sample to sample scatter is not expected. The best unirradiated and irradiated strength was obtained for material with the 150 nm thick carbon interfacial layer and the best strain to failure with the 1000 nm thick carbon layer.

In a comparison between composite and monolithic material, the fracture strength of the unirradiated composite material with the 150 nm carbon interface layer exceeded the fracture strength of the monolithic material while the strengths of the irradiated material were similar. For the composite with thicker carbon interfacial layers, the fracture strength of the irradiated composite materials was less than the monolithic material. The fracture strength

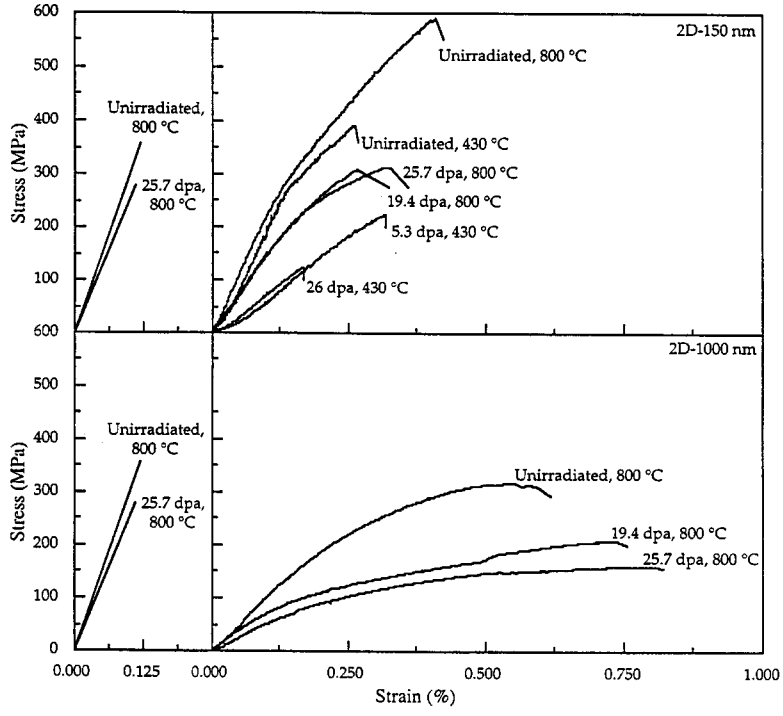

Fig. 13. Stress–strain response for several SiC/SiC composite materials irradiated and tested at 800°C with comparison to monolithic SiC.

of the irradiated composite material was equal to or less than the monolithic materials because the Nicalon® fibers had densified and are thus no longer in contact with the matrix and the matrix is highly microcracked. The shrinkage of the Nicalon® fibers with irradiation reduces their contribution to the load carrying capacity of the composite and the CVI β-SiC microstructure is more prone to microcracking than the polycrystalline monolithic material [46].

The fracture strengths are replotted as a function of fluence along with the addition of data at 500°C and 1200°C in Fig. 14. The curves are drawn to suggest a change in slope in the bend strength vs. dose at about 5 dpa because the shrinkage of the fibers occurs at less than 5 dpa, therefore; the largest drop in bend strength occurs in this fluence range. The optimum irradiated bend strength for these specimens occurred at 800°C.

Helium will be produced in SiC by transmutation at the rate of 50–150 appm/dpa depending on location within the fusion blanket. Information on the effects of He on the mechanical properties of SiC/SiC composites is limited although Hasegawa et al. [55] have evaluated the three-point bend strength of SiC/SiC implanted with 150 appm He. A 36 MeV He ion was used to implant He to a depth of about 470 μm at temperatures ranging from 400 to 800°C. No change was observed in the matrix cracking stress for He implanted samples but a 20% decrease in fracture strength was observed. This effect was related to the He since the damage level of 0.02 dpa is too low to produce a displacement damage effect on the strength. Sasaki et al. [56] evaluated the helium release from neutron irradiated SiC containing 0.1 wt% ^{10}B. Helium release was measured as a function of temperature for both polycrystalline and powder material and it was observed that a

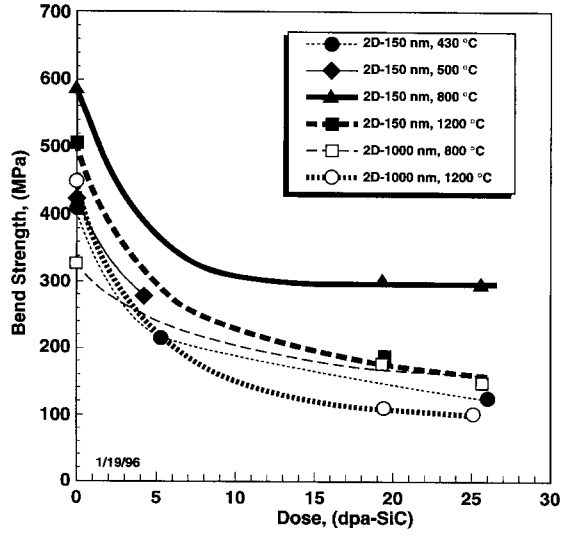

Fig. 14. Bend strength of several SiC/SiC composite materials as a function of irradiation dose for various irradiation and test temperatures.

small amount of He release occurred at a temperature as low as 500°C in the polycrystalline materials. However, the majority of the He release occurred at temperatures exceeding 1800°C because the He was trapped at grain boundaries. Release at 1800°C was explained by the interlinkage of He bubbles at the grain boundaries to form pores that interconnected with the surface. Grain boundary diffusion did not control the release of He trapped at grain boundaries. Based on observations of Sasaki et al., it is postulated that the He implanted by Hasegawa et al. [55] was sufficiently mobil at 400–800°C to diffuse to fiber/matrix or matrix/matrix interfaces and that this could explain the loss in strength. Further evaluation is needed to quantify the magnitude and mechanism of He effects in SiC/SiC composites.

Helium accumulation at grain boundaries has also been shown by Suzuki et al. [57] to enhance creep at temperatures above 1300°C. The presence of He bubbles at grain boundaries promoted diffusional creep of samples loaded in compression. Displacement damage also enhances the creep rate of SiC at temperatures within the projected temperature range of a SiC/SiC composite fusion blanket. Price [58] reported on the irradiation creep of chemical vapor deposited pyrolytic β-SiC strips irradiated at 780, 950, and 1130°C in a fast neutron spectrum to a maximum fluence of 7.7×10^{21} n/cm^2. While there are considerable uncertainties in this data, there is a significant increase in the creep rate of SiC during irradiation. Price's results show a temperature independent regime over the range of 780°C to 1100°C with a linear stress dependence. A creep rate enhancement of $10^3\times$ is possible at 1000°C and much greater at lower temperatures. Recently, Scholz [59] measured the torsion creep rate of SCS-6 fibers irradiated with 14 MeV deuterons. The SCS-6 fiber is produced by chemical vapor deposition on a carbon core so the fiber microstructure is very representative of the CVI matrix of the SiC/SiC composites. Scholz reported a significant irradiation creep rate at 600°C and a stress of 320 MPa. He also reported a flux dependence for the irradiation creep rate that was not previously measured and a linear stress dependence as reported by Price [58].

5. Fiber / interface / matrix options for radiation resistant composites

As stated previously, the primary routes being considered for radiation resistant composites focus on silicon carbide based materials. Therefore, only silicon carbide based fiber, interface and matrix options will be discussed in this section.

5.1. Fibers

Selection of a fiber for a radiation resistant CFCC will depend on similar factors to those considered for high-temperature CFCC applications plus the added requirement for stability in a neutron radiation environment. A key factor in the development of a radiation resistant SiC/SiC composite appears to be the condition where both the fiber and matrix radiation response closely matches that of β-SiC which exhibits limited swelling at temperature of 800–1000°C. Some of the newer fibers such as Hi-Nicalon® and DOW/NASA crystalline SiC approach the density and composition of β-SiC and also exhibit better swelling resistance than the more amorphous fibers.

Criteria for selection of fibers for high-temperature CFCCs presented by DiCarlo [7] are as follows: (1) high tensile strength, usually achieved with the absence of porosity and small grains; (2) creep resistance and strength retention at high-temperature, usually attained with stoichiometric compositions; (3) small diameter fibers for weaveability needed for making complex shapes and thin sections and (4) low cost, usually associated with cheap precursors, inexpensive facilities and rapid through-put.

The strength and fiber diameter for several silicon based fibers is shown along with processing method, composition, trade name, modulus, density and coefficient of expansion in Table 6, as presented by DiCarlo. The weaveable fibers, of primary interest for radiation resistant CFCCs, are those with fiber diameters of about 15 μm or less, i.e., Nicalon®, Hi-Nicalon® Tyranno, Tonen, HPZ, Fiberamic, DOW-Corning (D–C) and MER fibers. The strengths of these fibers at 25°C range from 1.5 to 3.5 GPa with the strength of the MER fiber not given. The fibers listed in Table 6 are all high-strength fibers although there is a factor of two difference in their strengths.

Creep resistance and strength retention can be evaluated with stress–rupture data such as that given in Fig. 15 for SiC and oxide fibers (Nextel 610, Altex, Almax and Saphikon). This figure, by DiCarlo, of the specific strength-temperature relationship for 1000 h rupture strength illustrates the greater creep resistance and strength retention of the silicon carbide based fibers relative to the

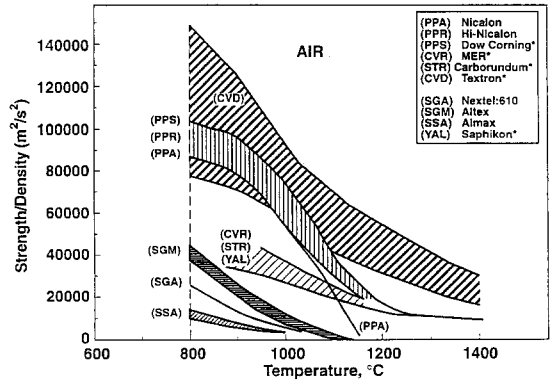

Fig. 15. Specific 1000 h stress rupture strength of oxide and SiC fibers.

alumina based fibers at temperatures below 1200°C. Some of this difference in specific stress rupture strength results from the approximately 30% higher density of the alumina based fibers but higher density accounts for only a small fraction of the difference. Also, for applications with operating temperatures between 800°C and 1200°C, the creep resistance and strength retention of the alumina fibers is considerably less than the silicon carbide based fibers.

The weighting factor given to material costs in selection of materials for a design varies with the application. Cost is a critical factor when there are many competing materials and the performance benefit is relatively small. Conversely, cost is less important when there are few competing materials and the performance benefit is large. A comparison of fiber costs and the current cost of SiC/SiC produced with Nicalon® fibers is shown in Fig. 16. Of the silicon based fibers, Nicalon® has the lowest cost because it is a commercial fiber while the others are developmental. Of the SiC fibers listed in Table 5, only Nicalon®, Tyranno and Tonen are commercially available. Hi-Nicalon® became commercially available in 1996 and the cost is expected to approach that of Nicalon® as the production volume increases.

5.2. Interfaces

The interface between fiber and matrix plays a critical role in the performance of CFCCs. The primary function of this interfacial layer is to transfer load to the fiber and provide a weak link for fiber pull-out prior to fiber fracture. Therefore, the interfacial layer must possess sufficient strength to transfer load to the fiber but must be weak enough to allow fiber/matrix debonding prior to fiber fracture. A strong interface bond results in a high fracture strength but a low fracture toughness and fracture behavior comparable to monolithic ceramics.

Carbon is the most common interfacial materials used in SiC/SiC composites. The structure of the carbon can be a mixture of amorphous and graphitic carbon where the amorphous layer is adjacent to the fiber and the graphitic carbon is adjacent to the matrix with the basal planes parallel to fiber axis. Fiber/matrix debonding occurs readily along the basal planes of the graphitic carbon. Debonding along the fiber/graphite or graphite/matrix interface is also a possibility. Therefore, several parameters such as bond strength at the fiber/carbon and carbon matrix interfaces and microstructure of the carbon layer are all important; however, the thickness of the carbon interface layer is sufficient to describe the properties of SiC/SiC. Lowden [4] has shown that for SiC/SiC made with Nicalon® fibers and CVI processing, the optimum carbon layer thickness is about 0.2 μm.

The fiber/matrix interfacial layer must also posses high temperature properties for applications at elevated temperatures in an oxidizing or corrosive environment. Tortorelli showed, in work reported by Jones et al. [60], that the fracture strength of SiC/SiC was reduced from 389 to 234 MPa following a $\frac{1}{4}$ h exposure to air at 950°C and to 71 MPa following an 800 h exposure. This decrease in fracture strength was directly related to the oxidation of carbon at the fiber/matrix interface. Jones et al. [60] also demonstrated that the subcritical crack velocity of a SiC/SiC composite with a carbon interface was increased by more than a factor of 10 in an argon +20 000 appm oxygen environment at 1100°C compared to high-purity argon.

Several alternative approaches are being evaluated to develop a stable high-temperature fiber/matrix interface. These approaches include the use of boron nitride in place of carbon, a multilayer interface of –SiC/C/SiC– where each layer is very thin, or a porous-defective SiC interfacial layer. Each of these interfacial layers offer different

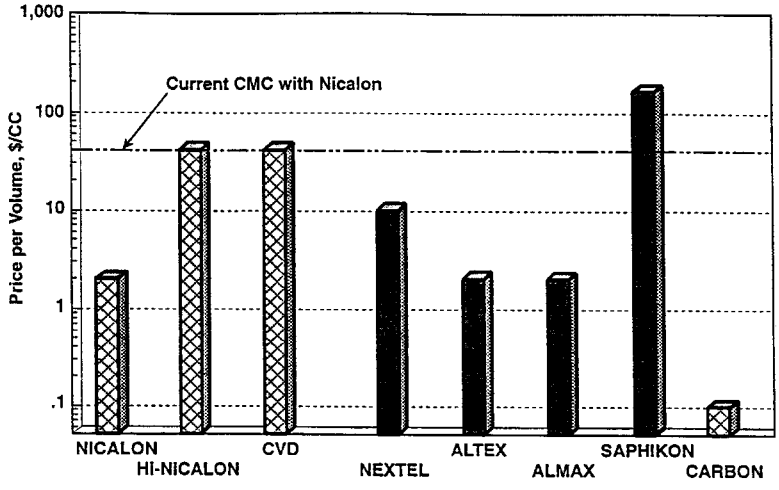

Fig. 16. Current costs for commercial fibers and processes for oxide and SiC fibers.

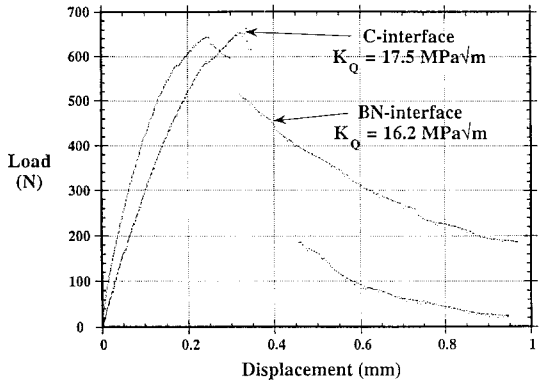

Fig. 17. Load deflection curves for SiC/SiC composites with C and BN layers in the Hi-Nicalon® fiber/matrix interfaces tested at 1100°C in high purity Ar.

high-temperature performance, but are at different stages of development. Boron nitride interfacial layers are not as readily available as carbon, but are developed to the state where composites with equal fracture strengths and fracture toughness to material with carbon interfaces can be obtained. For example, Fig. 17 shows that the load deflection curves at 1100°C for SiC/SiC with either carbon or boron nitride interface material exhibit virtually identical fracture strength and toughness values [13]. Boron nitride has the advantage of being more stable in oxidizing environments than carbon. This greater stability is demonstrated by subcritical crack growth results where the boron nitride interfacial layer resulted in a factor of five lower crack velocity than the carbon interfacial layer over oxygen concentrations of 2000 to 20 000 ppm [13]. The reaction rate of the interfacial carbon or boron nitride layer has

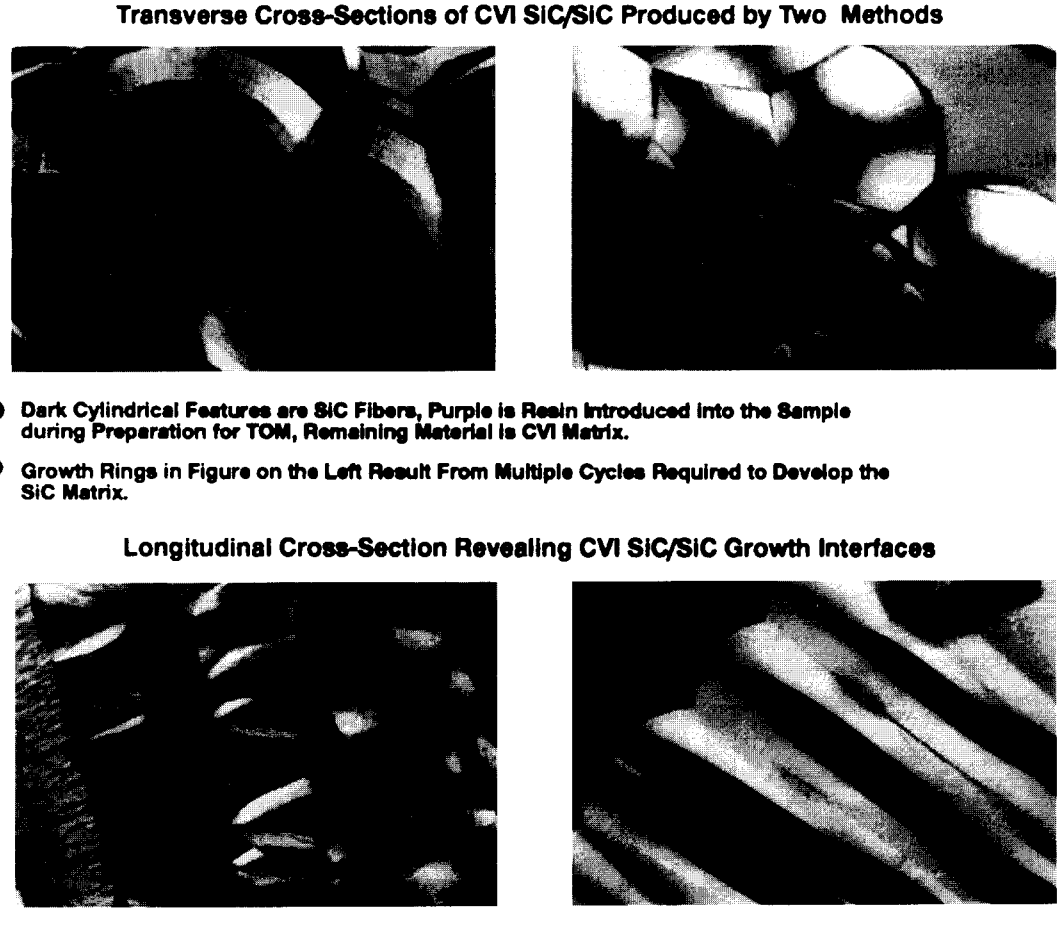

Fig. 18. Transmission optical micrograph of SiC/SiC composites produced by the thermal gradient and pressure gradient methods showing growth features present in the matrix material.

been shown to decrease if a glass layer forms in the interface. A glass layer has been shown to form [60] when the interface layer is thin and the oxygen activity is high. Therefore, the multi-layer interface of SiC/C/SiC/C/SiC has the potential for greater stability in oxidizing environments because of the thin carbon thickness. Porous or defective SiC interface layers can be applied by CVI to the fiber surface prior to formation of the matrix in a manner similar to the application of carbon or boron nitride. The properties of this interfacial layer must be controlled to achieve the desired load transfer and fiber/matrix debonding but the stability in oxidizing environments should be comparable to that of the matrix. An added benefit of reduced thermal stresses should result because of the similar coefficients of thermal expansion for the fiber, interface and matrix. Porous or defective SiC interfacial layers are being developed.

5.3. Matrixes

There are currently two primary routes for producing the matrix of CFCCs. These are the chemical vapor infiltration (CVI) route used by DuPont–Lanxide Composites, Inc., and the polymer-impregnation-pyrolysis (PIP) routes used by DOW/Kaiser Ceramic Composites. In addition, DuPont–Lanxide Corp. is attempting to develop the DIMOX process for producing SiC/SiC composites. Hot-pressing can be used to produce SiC/SiC with particular, whisker, chopped fibers or unidirectional fiber composites, but this is not a viable approach for 2D and 3D continuous fiber reinforcement. The high temperatures required to sinter SiC and high pressures needed for hiping or hot-presses cause damage to the reinforcing fibers while the addition of sintering aids reduces the high-temperature strength of the composite. Silicon melt infiltration process, as Silcomp™, is another option for producing composite materials but is not viable with polymer derived fibers because of the high processing temperatures.

A composite is produced by CVI by infiltrating a carbon–silicon containing gas such as methyltrichlorsilane into a fiber preform at elevated temperatures. Besmann [61] summarizes the five types of CVI processes as follows: (1) isothermal, reagents surround the preform and enters the preform via diffusion; (2) thermal gradient, reagents contact the cold surface of the preform and enter via diffusion with the highest reaction rate proceeding at the hot surface of the preform; (3) isothermal-forced flow, same as No. 1 with a pressure gradient across the preform; (4) thermal gradient-forced flow, same as No. 2 with a pressure gradient across the preform and (5) pulsed flow, reagents flow into and out of the preform as a result of cyclic evacuation and back-filling of the reaction chamber. DuPont–Lanxide Composites and SEP in France use process No. 1, while Oak Ridge National Laboratory and General Atomics have chambers that produce material with process No. 4. The advantage of process No. 4, relative to No. 1, is that the process can be completed in a single cycle. Process No. 1 requires multiple cycles where the material is removed and treated because the reaction proceeds more rapidly at the surface and the deposition rate at internal surfaces is reduced. However, process No. 1 lends itself to large reaction chambers and the production of large volumes of material with each batch. All five CVI processes result in a material with a 10% to 15% porosity and have the advantage of being a relatively low temperature process that minimizes damage to fibers which results in minimal residual stress.

The resulting matrix produced by CVI is β-SiC with a variety of growth features as shown in Fig. 18. This figure shows the growth rings for the discontinuous process No. 1 and continuous matrix growth produced by process No. 4. Other features in this micrograph include growth interfaces, where the matrix growth front emanating outward from the fibers come into contact, and selected nucleation and growth from small features on the fiber surface.

A flow diagram of the PIP process used by Kaiser Ceramic Composites is shown in Fig. 19. In this process, the matrix polymer is impregnated into the fiber preform, cured and then pyrolyzed at temperatures greater than 1000°C. Subsequent impregnation and pyrolysis steps are conducted to reduce the porosity and increase the density. A material with as little as 5% porosity is possible, but this requires several PIP cycles. The final structure of this material depends on the pyrolysis temperature and conditions, but the matrix structure closely resembles that of polymer derived ceramic fibers such as Nicalon®.

The directed metal oxidation (DIMOX) process devel-

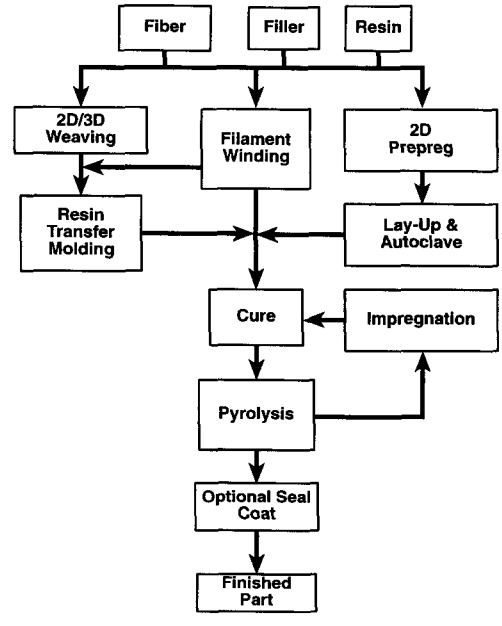

Fig. 19. Schematic of the polymer-impregnation-pyrolosis process used by Kaiser Ceramic Composites.

oped by the DuPont-Lanxide Corp. Produces a ceramic matrix by the oxidation of a liquid metal. In the case of SiC, liquid Si is reacted with a 'carbon rich gas' to form SiC and residual Si. This reaction has been demonstrated with CF_4 as the 'carbon gas' and Fe or Mn additions to aid wicking of the molten Si through a particulate reinforcement. This process has the advantage relative to CVI and PIP of producing a composite with little or no porosity and being relatively low-cost. The residual Si and wicking additives, Fe or Mn, are potential problems for this material in a radiation environment. The 1700°C processing temperature required to melt the Si is also potentially a problem for many polymer derived SiC fibers.

6. Summary, key issues and future directions

Composite materials made with continuous SiC fibers are being considered for fusion energy systems and advanced reactor applications where radiation stability is a primary performance criteria. The ARIES-I Tokamak Reactor Study was conducted with SiC/SiC as the primary structural material for the first wall and blanket. This study identified the promise and major feasibility issues of this material for this application. This design demonstrated that SiC/SiC is a viable structural material for fusion applications based on modest extrapolations from currently available SiC/SiC material. The issues raised by this and subsequent studies [62] include hermetic properties, thermal conductivity, radiation stability, transmutation effects, thermal shock and fatigue, chemical compatibility, creep and subcritical crack growth and joining methodology.

A review of the properties of SiC/SiC composites, with an emphasis on those listed as feasibility issues in the ARIES-I design study, helped to identify where improvements may be needed. The thermal shock and low-cycle fatigue properties of SiC/SiC are very good while there is insufficient information regarding the hermetic properties and transmutation effects to draw specific conclusions. Clear improvements will be needed in the thermal conductivity and radiation stability for applications in fusion energy systems. The 'engineerable' nature of these materials could be a tremendous benefit in their development. Evaluations can be conducted on a subelement of the material, such as the fibers, in parallel with development work on the composite and the results, i.e., improved fibers, included in the latest material.

Radiation stability is a significant issue for the application of SiC/SiC in a neutron irradiation environment. Beta SiC exhibits excellent dimensional stability in the temperature range of 800 to 1000°C and this stability is also demonstrated in crystalline SiC fibers. Also, the closer that polymer derived SiC fibers are to crystallinity the better their radiation stability. Further research is in progress to understand the factors affecting their instability and to identify the most stable fibers.

The development of radiation resistant ceramic matrix composites is in an early state. There have been no studies with materials tailored for radiation resistance. Several options were suggested at this workshop for improved radiation resistance. These options included: (1) crystalline, stoichiometric fibers; (2) spinel $MgO \cdot nAl_2O_3$; (3) alternate interfaces such as layered, porous SiC, spinel and metal oxides; (4) alternate matrix processing routes such as DIMOX and slurry infiltration routes and (5) alternate fiber architectures. A considerable research effort is needed to identify the optimum radiation resistant material and to obtain a comprehensive property database on both the unirradiated and irradiated material. Clearly, collaborations among those interested in the application of these materials will be necessary to accomplish this goal.

A number of issues, beyond those raised by the ARIES-I study, regarding the application of ceramic matrix composites for a radiation environment were identified. These issues include: (1) development of a sufficient database for the unirradiated and irradiated materials including properties such as tensile, fracture, creep, fatigue, thermal shock, and thermal conductivity; (2) material cost; (3) concern about hermetic properties for pressure boundary applications; (4) joining methodology including radiation resistant joining materials and the ability to perform field joining; (5) a standardized method for calculating radiation displacement damage; and (6) a need for an accepted design criteria for composite materials. Some specific issues for fusion applications are: (1) the high gaseous transmutation rates and their impact on properties, (2) low activation issues associated with ^{26}Al production, and (3) concerns about hot atom chemistry (p, d, T) associated with plasma–wall interactions.

The development of radiation resistant ceramic matrix composites will be a major undertaking that is beyond the resources of any one user. Therefore, collaborations between several parties were recommended. Some specific topics recommended for collaborations include: (1) irradiation studies; (2) modeling and analysis of radiation induced amorphization; (3) small angle neutron scattering studies of radiation damage; (4) fundamentals of displacement damage in covalent and ionic systems; (5) utilization of electron microscopy user centers; and (6) development of design criteria.

References

[1] The ARIES-I Tokamak Reactor Study, Final Report, UCLA-PPG-1323 (1991).
[2] J.J. Kibler, Composite Laminte Analysis System (Class), Materials Sciences (ASM International, Metals Park, OH, 1987).
[3] P. Fenici, H.W. Scholz, J. Nucl. Mater. 212–215 (1994) 60.
[4] R.A. Lowden, ORNL/TM-11039 (Mar. 1989).
[5] R.M. Laine, Chem. Mater. 5 (1993) 260.

[6] C.R. Blanchard, S. Schwab, J. Am. Ceram. Soc. 77 (1994) 1729.
[7] J.A. DiCarlo, High-Temperature Structural Fibers-Status and Needs, NASA TM (1991) 105174.
[8] A.G. Evans, R.M. McMeeking, Acta Metall. 34 (1986) 2435.
[9] D.B. Marshall, B.N. Cox, A.G. Evans, Acta Metall. 33 (1985) 2013.
[10] A.G. Evans, J. Am. Ceram. Soc. 73 (1990) 187–206.
[11] S.M. Wiederhorn, B.J. Hockey, 'High temperature degradation of structural ceramics', presented at the 7th World Ceramics Congr., Montecatini Terme, Italy, June 24–30, 1990.
[12] J.W. Holmes, J.L. Chermant, Creep Behavior of Fiber-Reinforced Ceramic Matrix Composites in High Temperature Ceramic Matrix Composites, 6th Eur. Conf. on Composite Materials, Sept. 1993, Bordeaux (Woodhead, Abington Hall, Abington, Cambridge, UK) p. 633.
[13] C.H. Henager Jr., R.H. Jones, J. Am Ceram. Soc. 77 (1994) 2381.
[14] C.R. Jones, C.H. Henager Jr., R.H. Jones, Scr. Metall. Mater. 33 (1995) 2067.
[15] J.L. Henshall, D.J. Rowcliffe, J.W. Edington, J. Am. Ceram. Soc. 62 (1&2) (1979) 36.
[16] J.L. Henshall, Res. Mech. 1 (1980) 229.
[17] J.L. Henshall, in: Advances in Fracture Research (Fracture 81), ed. D. Francois (Pergamon, New York, 1981) p. 1541.
[18] C.H. Henager Jr., R.H. Jones, Ceram. Trans. 10 (1990) 197.
[19] E. Bakis and W.W. Stinchcomb, in: Composite Materials: Fatigue, Fracture, ASTM STP 907, ed H.T. Hahn (American Society for Testing and Materials, Philadelphia, PA, 1986) p. 314.
[20] J.W. Holmes, J. Am. Ceram. Soc. 74 (1991) 1639.
[21] D. Rouby, P. Reynaud, in: Proc. Conf. on High Temperature Ceramic Matrix Composites held at the 6th Eur. Conf. on Composite Materials, Bordeaux, Sept. 20–24, 1993, p. 499.
[22] R.H. Jones, C.H. Henager Jr., Fusion Reactor Materials Semiannual Progress Report for period ending March 31, DOE/ER-0313/14, 1993, p. 451.
[23] J.W. Holmes, Y.H. Park, J.W. Jones, J. Am. Ceram. Soc. 76 (1993) 1281.
[24] W.J. Lee, E.D. Case, Mater. Sci. Eng. A119 (1989) 113.
[25] Y. Kagawa, N. Kurosawa, T. Kishi, Y. Tanaka, Y. Iamai, H. Ischikawa, Ceram. Eng. Sci. Proc. 10 (1989) 1327.
[26] A.J. Eckel, J.Z. Gyekenyesi, T.P. Halso, E.R. Generazio, Thermal Shock of Fiber Reinforced Ceramic Matrix Composites, National Aeronautic and Space Administration, NASA TM-103777, 1991.
[27] H. Wang, R. Singh, Ceramic Engineering and Science Proc., 1994 Cocoa Beach Meeting, in press.
[28] E. Pearson, T. Takai, T. Halicioglu, W. Tiller, J. Cryst. Growth 70 (1984) 33.
[29] M. Baskes, J. Nelson, A. Wright, Phys. Rev. B40 (1989) 6085.
[30] J. Tersoff, Phys. Rev. B37 (1988) 6991.
[31] D.M. Parkin, C.A. Coulter, J. Nucl. Mater. 101 (1981) 261.
[32] D.M. Parkin, C.A. Coulter, J. Nucl. Mater. 103&104 (1981) 1315.
[33] D.M. Parkin, C.A. Coulter, J. Nucl. Mater. 117 (1983) 340.
[34] J.F. Ziegler, J.P. Biersack, U. Littmark, The Stopping and Range of Ions in Solids (Pergamon, New York, 1985).
[35] W.J. Weber, R.E. Williford, K.E. Sickafus, Proc. Symp. on Radiation Materials Science in Technology Applications, TMS Annual Meeting, February 4–8, 1996, Anaheim, CA, J. Nucl. Mater. 244 (1997) 205.
[36] S.J. Zinkle, C. Kinoshita, Proc. of the Int. Workshop on Defect Production, Accumulation and Materials Performance in Irradiation Environment, Davos, Switzerland, Oct. 2–8, 1996. J. Nucl. Mater, to be published.
[37] A. El-Azab, N.M. Ghoniem, J. Nucl. Mater. 191–194 (1992) 1110.
[38] J. Wong, T. Diaz de la Rubia, M.W. Guinan, M. Tobin, J. Perlado, A.S. Perez, J. Sanz, J. Nucl. Mater. 212–215 (1994) 143.
[39] H. Huang, N.M. Ghoniem, J.K. Wong, M.I. Baskes, Mater. Sci. Eng. 3 (1995) 615.
[40] H. Huang, N.M. Ghoniem, J. Nucl. Mater. 199 (1993) 221.
[41] M. Hon, R. Davis, J. Mater. Sci. 14 (1979) 2411.
[42] M. Hon, R. Davis, J. Mater. Sci. 15 (1980) 2073.
[43] H. Inui, H. Mori, A. Suzuki, H. Fujita, Philos. Mag. B65 (1992) 1.
[44] W.J. Weber, L.M. Wang, Nucl. Inst. Meth. B106 (1995) 298.
[45] S.D. Harrison, J.C. Corelli, J. Nucl. Mater. 99 (1981) 203.
[46] G.W. Hollenberg, C.H. Henager Jr., G.E. Youngblood, D.J. Trimble, S.A. Simonson, G.A. Newsome, E. Lewis, J. Nucl. Mater. 219 (1995) 70.
[47] M.C. Osborne, L.L. Snead, D. Steiner, J. Nucl. Mater. 219 (1995) 63.
[48] L.L. Snead, M. Osborne, K.L. More, J. Mater. Res. 10 (1995) 736.
[49] A. Hasegawa, G.E. Youngblood, R.H. Jones, Fusion Materials Semiannual Progress Report for period ending Dec. 31, 1995, DOE/ER-031/19, p. 101.
[50] J.E. Palentine, J. Nucl. Mater. 92 (1980) 43.
[51] J.E. Palentine, J. Nucl. Mater. 61 (1976) 243.
[52] R.J. Price, J. Nucl. Mater. 48 (1973) 47.
[53] M. Rohde, J. Nucl. Mater. 182 (1991) 87.
[54] C.W. Lee, F.J. Pineau, J.C. Corelli, J. Nucl. Mater. 108&109 (1982) 678.
[55] A. Hasegawa, M. Saito, K. Abe, R.H. Jones, in: Proc. of IEA Int. Workshop on SiC/SiC Ceramic Composites for Fusion Structural Applications, Oct. 28–29, 1996, Ispra, Italy.
[56] K. Sasaki, T. Yano, T. Maruyama, T. Iseki, J. Nucl Mater. 179 (1991) 407.
[57] T. Suzuki, T. Yano, T. Mori, H. Miyasaki, T. Iseki, Fusion Technol. 27 (1995) 314.
[58] R.J. Price, Nucl. Technol. 35 (1977) 320.
[59] R. Scholz, in: Proc. IEA Int. Workshop on SiC/SiC Ceramic Composites for Fusion Structural Applications, Oct. 28–29, 1996, Ispra, Italy, p. 147.
[60] R.H. Jones, C.H. Henager Jr., P.F. Tortorelli, J. Organomet. 45 (12) (1993) 26.
[61] T.M. Besmann, Ceram. Trans. 58 (1995) 1.
[62] R.H. Jones, C.H. Henager Jr., J. Nucl. Mater. 212 (1994) 830.